Rotational Spectrum and Inversion Motions in the Neon−Dimethyl Sulfide Complex

Sean A. Peebles* and Rebecca A. Peebles

Department of Chemistry, Eastern Illinois University, 600 Lincoln Avenue, Charleston, Illinois 61920

Yoshio Tatamitani and Yoshiyuki Kawashima

Department of Applied Chemistry, Kanagawa Institute of Technology, Atsugi, Kanagawa 240-0292 Japan

Received: February 26, 2006; In Final Form: April 3, 2006

The rotational spectra of the ^{20}Ne and ^{22}Ne isotopomers of the Ne-dimethyl sulfide (DMS) rare gas dimer have been measured by Fourier transform microwave spectroscopy. MP2/6-311++G(2d,2p) calculations, and the experimental spectroscopic data, suggest a structure of C_s symmetry in which the Ne atom lies above the heavy atom plane of the DMS (in the σ_v plane which bisects the CSC angle). Experimental rotational constants are consistent with a S···Ne distance of 3.943(6) Å and a (cm···S···Ne) angle of 63.2(6)° (where cm is the center of mass of DMS). A motion of the Ne atom from one side of the DMS to the other gives rise to inversion splittings of around 3 MHz in the *c*-type transitions. An ab initio potential energy surface calculation has allowed examination of several possible tunneling pathways, and suggests a barrier of between 20 and 40 cm^{-1} for the inversion motion, depending on the tunneling pathway taken by the Ne. Dipole moment measurements are consistent with both the experimental and ab initio structures.

Introduction

Although dimethyl sulfide (DMS) is considered to be the largest natural source of sulfur in the atmosphere and is an important component in the marine environment, studies of DMS complexes by high resolution spectroscopy are rare. Indeed, Novick's bibliography of weakly bound complexes lists only one unpublished microwave study of a complex of DMS (Ar−DMS).[1,2] Kinetics studies utilizing techniques such as cavity ring-down spectroscopy on the complex DMS−Cl atom[3] do exist, but there is a lack of structural determinations of the weakly bound complexes of this molecule. As part of a systematic study that aims to characterize the importance of C−H hydrogen bonding interactions, we initiated a study of complexes of DMS to provide structural comparisons with complexes of dimethyl ether (DME), studies of which are far more numerous in the literature.[4] DME is a good candidate for formation of C−H hydrogen bonding interactions, because the methyl group protons are sufficiently acidic to form C−H···X interactions (where X is a proton acceptor); for example, the dimethyl ether dimer[5] exhibits three C−H···O interactions. The replacement of the oxygen atom in DME with a sulfur atom in DMS leads to a very different electronic environment and the much lower electronegativity and weaker acceptor properties of sulfur compared to oxygen will undoubtedly play an important role in the intermolecular interactions of DMS. It is therefore of interest to observe the effects on the structures of weak complexes that will arise from the differences in the electronic environments in analogous DME and DMS complexes.

This paper reports the assignment of the spectra of two isotopomers of the Ne−DMS weakly bound complex, identified during a search for the DMS−OCS complex. Ab initio calculations at the MP2/6-311++G(2d,2p) level have been used to confirm the structure and, via a calculated potential energy surface, to investigate the possible tunneling pathways for the inversion motion of the Ne atom. Structural comparisons with the Ne−DME complex[6] will also be presented.

Experimental Section

The rotational spectra of the ^{20}Ne−DMS and ^{22}Ne−DMS species in the frequency range 7−13 GHz were observed initially on a Balle-Flygare Fourier transform microwave spectrometer[7] at Eastern Illinois University; this spectrometer has been described in detail previously.[8,9] Additional transitions were subsequently measured on a similar instrument[10,11] at the Kanagawa Institute of Technology, considerably extending the frequency range to 3.7−24.1 GHz. The data acquisition system of this instrument has been recently improved by introducing the computer programming software LabVIEW. The data acquisition system now serves in three ways, namely, as a multifunction input/output (I/O) unit, a timing I/O unit, and a digitizer. The first function is used as an analog/digital converter of slow sampling speed, the second function generates timing pulses for the switches and the nozzle driver, and the last function takes free-induction decay signals with the sampling speed of 64 MS/s and 14-bit resolution. The frequency reproducibility of the spectrometer is 2 kHz.

Because the spectrum of the Ne−DMS complex was originally identified during searches for the DMS−OCS dimer, the initial searches were carried out with mixtures of 1.5% each of DMS (Sigma-Aldrich) and OCS (97.5+%, Sigma-Aldrich) in He/Ne (17.5% He: 82.5% Ne, BOC Gases) at backing pressures up to 2.5 atm; this mixture was expanded through a 0.8 mm General Valve Series 9 pulsed nozzle into the vacuum chamber to generate the complex. Successive dilutions of the sample mixture gave increased intensity of the Ne−DMS transitions, and the optimum concentration is likely considerably less than 1.5% DMS. The measurements in Japan used a sample of

* Corresponding author. E-mail: sapeebles@eiu.edu. Phone: (217) 581-2679. Fax: (217) 581-6613.

10.1021/jp061219o CCC: $33.50
Published on Web 05/11/2006

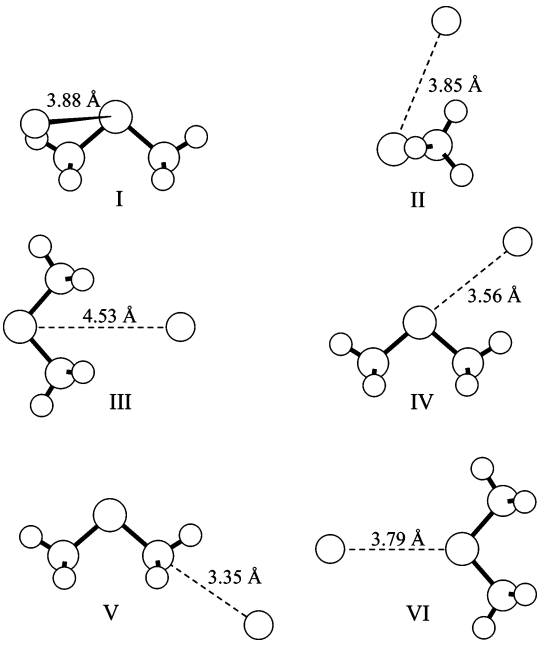

Figure 1. Six stationary points obtained from ab initio optimizations of Ne−DMS at the MP2/6-311++G(2d,2p) level. Structures are labeled in order of decreasing stability of the BSSE and ZPE uncorrected energy. Structure I has C_1 symmetry, II, IV and V have C_s symmetry, and III and VI have C_{2v} symmetry.

∼0.5% DMS with a backing pressure of pure Ne of 5−6 atm which resulted in transitions of comparable intensity. Stark effect experiments (for dipole moment measurements and for confirmation of quantum number assignments) were carried out at Eastern Illinois University by the application of voltages up to ±5 kV to a pair of steel mesh plates separated by 31 cm and situated within the Fabry−Perot cavity. Electric field calibration was carried out by measurement of the $J = 1 \leftarrow 0$ transition of OCS, assuming a dipole moment of 0.71521 D.[12]

Spectra, Structure and Binding. Two doublets (each split by between 2.5 and 3 MHz) of similar intensity and centered at 8034 and 7905 MHz were observed in the initial search and were quickly identified by their Stark shifts as the $J = 1_{10} \leftarrow 0_{00}$ transition for the ^{20}Ne−DMS and ^{22}Ne−DMS isotopomers. A search in the 12 GHz region for the $J = 2_{11} \leftarrow 1_{01}$ transition for the ^{20}Ne and ^{22}Ne isotopomers revealed doublets at 12296 and 11915 MHz both showing similar 3 MHz splittings despite the relatively large change in tunneling mass on going from ^{20}Ne to ^{22}Ne (similarly small variations in the isotopic splittings were observed previously in the neon-cyclopropane complex[13]). Interestingly, the intensities of the ^{20}Ne and ^{22}Ne isotopic spectra were comparable despite the 9:1 ^{20}Ne:^{22}Ne ratio in nature. Similar intensity enhancements of the ^{22}Ne containing isotopomers have been observed in other complexes, such as Ne_2−Ar,[14] Ne_2−N_2O[15] and Ne_2−OCS.[16] The isotopic shifts in the transition frequencies between the ^{20}Ne and ^{22}Ne isotopomers were consistent with those calculated from a Ne−DMS structure obtained from ab initio calculations in which the Ne atom lies above the C−S−C plane of the DMS (to be discussed below; see structure II in Figure 1). Using the $1_{10} \leftarrow 0_{00}$ and $2_{11} \leftarrow 1_{01}$ transition frequencies and assuming a P_{bb} similar to the P_{aa} value of the DMS monomer (P_{aa}(DMS) = 63.16202(6) u Å^2),[17] as expected if the Ne is in the CSC bisector plane of the DMS, the remaining *c*-type transitions were predicted and easily located. Given the small (∼3 MHz) inversion splitting, identification of the inversion doublets was straightforward. The most intense of the *c*-type transitions were observed with signal-to-noise ratios of 75 in 30 gas pulses. The significantly lower intensity *a*-type transitions were located easily on the basis of a fit of the previously assigned *c*-type lines but showed inversion splittings considerably smaller than were observed for the *c*-type transitions. The *a*-type lines also showed indications of additional fine splittings, presumably arising from internal motion of the methyl groups of dimethyl sulfide. These splittings increased in complexity and magnitude with increasing J and K_a, but given their lower intensity and small magnitude, no further analysis of this fine structure was carried out.

Fitting of the observed transitions utilized Pickett's SPFIT program,[18] using the Watson *A*-reduction Hamiltonian in the I^r representation,[19] with the coupled Hamiltonian of Pickett[20] shown in

$$H = H_R(0^+) + H_R(0^-) + H_{CD} + \Delta E \qquad (1)$$

where $H_R(0^+)$ and $H_R(0^-)$ are rigid rotor Hamiltonians describing the 0^+ and 0^- tunneling substates, respectively, H_{CD} provides centrifugal distortion corrections and ΔE is the energy difference between the 0^+ and 0^- states; 0^+ and 0^- refer to the tunneling ground and first excited states. Table 1 lists the observed transition frequencies and the residuals from the last cycle of the fitting process and Table 2 gives the resulting spectroscopic constants. It is noteworthy that the value for the tunneling frequency (ΔE) in the ^{20}Ne isotopomer is slightly higher than that in the ^{22}Ne isotopomer, consistent with the larger reduced mass in the ^{22}Ne species. Note that an average value of the *A* rotational constant of the two tunneling states was fit for the ^{22}Ne−DMS species to reduce correlation problems (which were problematic given the reduced data set).

Attempts to locate the Ne−^{34}S$(CH_3)_2$ species in natural abundance were also made. Although some candidates for the $1_{10} \leftarrow 0_{00}$ and $2_{11} \leftarrow 1_{01}$ transitions (displaying qualitatively correct Stark effects) were identified in the predicted regions, their very low intensities precluded further study; an isotopically enriched sample (not presently commercially available) will be necessary for unambiguous assignment of this species.

The planar moments (P_{bb}) for the two isotopomers (P_{bb}(^{20}Ne−DMS) = 63.02726(12) u Å^2, P_{bb}(^{22}Ne−DMS) = 63.04315(19) u Å^2) are consistent with the location of the Ne atom in the CSC bisector plane of DMS because they are very close to the P_{aa} moment of DMS monomer (63.16202(6) u Å^2).[17] Once the Ne atom is determined to lie in this plane, only two structural parameters are required to describe the structure of Ne−DMS: the S···Ne separation (R) and the angle α (defined as (cm···S···Ne), where cm is the center of mass of DMS; see Figure 2). The average moments of inertia for each of the two isotopomers were least-squares fitted to the parameters R and α using the STRFITQ program.[21] The DMS monomer geometry was held fixed at the literature value[17] during this fitting process. The structural parameters that result are shown in Table 3. Fitting each of the isotopic species individually or both species simultaneously gave essentially identical results that agreed within the tabulated uncertainties.

Table 3 shows that two structures are consistent with the rotational constants obtained for the ^{20}Ne and ^{22}Ne species. These two structures have identical center of mass separations (R_{CM}, Table 3) but differ in the horizontal projection of the Ne atom's position onto the C_2 axis of the DMS (Figure 3). Because the results of the ab initio calculations only identified the geometry described by the parameters in the first column of Table 3 as a stationary point, we favor the structure in which the Ne atom is located further back toward the methyl groups of DMS (structure II, Figures 1 and 3).

TABLE 1: Rotational Transition Frequencies (MHz) and Residuals for the ^{20}Ne−DMS and ^{22}Ne−DMS Species

		^{20}Ne−DMS				^{22}Ne−DMS			
$J_{K_aK_c}'$	$J_{K_aK_c}''$	$0^+ \leftarrow 0^+$	$\Delta\nu^a$	$0^- \leftarrow 0^-$	$\Delta\nu$	$0^+ \leftarrow 0^+$	$\Delta\nu$	$0^- \leftarrow 0^-$	$\Delta\nu$
				a-Type Transitions					
2_{12}	1_{11}	7594.7843	−0.0028	7594.7725	−0.0070				
2_{02}	1_{01}	7888.5289	−0.0056	7888.4559	−0.0023	7452.2163	−0.0061	7452.1632	−0.0042
2_{11}	1_{10}	8215.8902	0.0000	8215.7646	−0.0036	7742.2291	−0.0028	7742.1456	0.0030
3_{13}	2_{12}	11378.9402	0.0002	11378.9278	−0.0016	10771.2969	0.0020	10771.2969	0.0020
3_{03}	2_{02}	11784.8078	0.0013	11784.7133	0.0010	11140.7156	0.0007	11140.6520	0.0043
3_{12}	2_{11}	12309.1904	0.0042	12309.0199	0.0057	11601.6799	0.0042	11601.5491	0.0041
4_{14}	3_{13}	15148.1350	0.0008	15148.1208	−0.0001				
4_{04}	3_{03}	15625.9787	0.0074	15625.8872	0.0077				
4_{23}	3_{22}	15779.5215	0.0044	15779.4283	0.0038				
4_{22}	3_{21}	15958.6037	0.0051	15958.4764	0.0036				
4_{13}	3_{12}	16383.9900	0.0011	16383.7750	−0.0037				
5_{15}	4_{14}	18898.8618	−0.0067	18898.8441	−0.0077				
5_{05}	4_{04}	19400.8098	−0.0046	19400.7424	−0.0017				
		^{20}Ne−DMS				^{22}Ne−DMS			
$J_{K_aK_c}'$	$J_{K_aK_c}''$	$0^+ \leftarrow 0^-$	$\Delta\nu$	$0^- \leftarrow 0^+$	$\Delta\nu$	$0^+ \leftarrow 0^-$	$\Delta\nu$	$0^- \leftarrow 0^+$	$\Delta\nu$
				c-Type Transitions					
1_{11}	1_{01}	3768.6158	0.0032	3771.8238	0.0015	3893.9602	−0.0021	3896.7576	−0.0009
1_{10}	0_{00}	8033.2283	−0.0007	8036.4177	−0.0043	7904.8958	−0.0015	7907.6768	−0.0023
2_{12}	2_{02}	3474.9409	−0.0006	3478.0701	0.0028	3629.7214	−0.0031	3632.4670	0.0007
2_{11}	1_{01}	12295.1978	−0.0060	12298.2259	−0.0064	11913.4721	0.0027	11916.1347	0.0033
2_{21}	2_{11}	11309.3252	0.0009	11312.1289	0.0022	11684.8618	−0.0002	11687.3254	−0.0062
2_{20}	2_{12}	12259.2637	0.0036	12262.2352	0.0032	12530.4996	0.0028	12533.1005	0.0021
2_{20}	1_{10}	19543.4017	0.0038	19546.3221	0.0040	19441.1961	−0.0006	19443.7568	0.0040
2_{21}	1_{11}	19835.7347	0.0004	19838.7165	−0.0014	19704.2341	−0.0008	19706.8399	0.0011
3_{03}	2_{11}	7375.1072	−0.0015	7377.9719	0.0052	6676.8104	0.0045	6679.3454	−0.0003
3_{22}	3_{12}	10848.9260	−0.0046	10851.4962	−0.0043	11272.5875	0.0054	11274.8826	0.0112
3_{21}	3_{13}	12801.7139	−0.0005	12804.6023	0.0023	13004.9609	0.0042	13007.5009	−0.0006
3_{12}	2_{02}	16715.9341	0.0023	16718.7187	0.0067	16062.9819	0.0042	16065.4577	0.0037
3_{21}	2_{11}	23249.0116	−0.0017	23251.7321	−0.0038	22944.8075	−0.0033	22947.2126	−0.0043
3_{22}	2_{12}	24089.5751	−0.0002	24092.4891	−0.0017	23705.5616	−0.0082	23708.1165	−0.0081
4_{23}	4_{13}	10244.6701	0.0011	10246.9381	0.0020	10730.2292	0.0012	10732.2621	−0.0006
4_{04}	3_{12}	10692.0688	0.0031	10694.6479	−0.0121	9860.8232	−0.0003	9863.1708	−0.0002
4_{22}	4_{14}					13705.8604	−0.0003	13708.3044	0.0013
4_{32}	4_{22}	19406.0611	−0.0004	19407.4353	−0.0004				
4_{13}	3_{03}	21315.2052	−0.0032	21317.6838	−0.0004	20368.8192	−0.0006	20371.0600	−0.0003
5_{05}	4_{13}	13709.1025	0.0010	13711.4203	0.0051				
5_{23}	5_{15}	14755.1620	−0.0010	14757.7026	−0.0007				
6_{06}	5_{14}	16384.5808	0.0014	16386.6197	0.0009				

[a] $\Delta\nu = \nu_{obs} - \nu_{calc}$ where ν_{calc} is calculated from the constants in Table 2.

Single isotopic substitution of ^{20}Ne by ^{22}Ne allowed the calculation of Kraitchman coordinates[22] for the Ne atom. This calculation gives values of $|a| = 2.7705$ Å, $|b| = 0.0944$ Å, $|c| = 0.0726$ Å (again based on fitting the average of the rotational constants obtained for the 0^+ and 0^- states). These coordinates may be compared to the coordinates obtained from the least-squares fit of the moments of inertia which gave $a = 2.8075$ Å, $b = 0.0000$ Å, $c = \pm 0.0972$ Å (where the two signs of the *c* coordinate reflect the two possible structures that are consistent with the inertial data; see Figure 3). Uncertainties in the Kraitchman coordinates are estimated to be on the order of ±0.0001 Å. The *a*-coordinate is in excellent agreement and the small magnitude of the *c*-coordinate is also reproduced reasonably well. The slightly nonzero value of the *b*-coordinate (expected to be zero in the presence of C_s symmetry) is not especially problematic, particularly in light of the low energy vibration that takes the Ne out of the symmetry plane (between the two equivalent minima labeled as I in Figure 1). In addition, the difficulties in precise determination of coordinates for atoms lying close to an inertial axis (due to incomplete cancellation of vibrational effects of the two isotopomers) are well-known.

Using the pseudodiatomic approximation,[23] and assuming that the *a*-axis of the complex is roughly coincident with the cm···Ne bond, it is possible to calculate a value for the weak bond stretching force constant (k_s) for Ne−DMS using

$$k_s = \frac{16\pi^4(\mu R_{CM})^2[4B^4 + 4C^4 - (B-C)^2(B+C)^2]}{hD_J} \quad (2)$$

where μ is the reduced mass of the complex, R_{CM} is the center of mass separation, *B* and *C* are rotational constants of the dimer and D_J is the Watson *S*-reduction centrifugal distortion constant. The resulting value of k_s (=0.573(3) N m^{-1}) can then be used to estimate a value for the binding energy of the complex (E_B), using an expression derived from a Taylor series expansion of a Lennard-Jones 6-12 potential[24]

$$E_B = \frac{1}{72}k_s{R_{CM}}^2 \quad (3)$$

It is noteworthy that the values of $k_s = 0.573(3)$ N m^{-1} and $E_B = 0.66(15)$ kJ mol^{-1} are both about half of the magnitude calculated for the Ne−DME complex ($k_s = 1.0$ N m^{-1} and $E_B = 1.0$ kJ mol^{-1}),[6] suggesting a slightly weaker binding in the Ne−DMS complex compared to the Ne−DME complex.[6] The quoted errors in k_s and E_B are propagated from the errors in the spectroscopic constants given in Table 2.

TABLE 2: Fitted Spectroscopic Constants for the ^{20}Ne−DMS and ^{22}Ne−DMS Isotopomers[a]

parameter	^{20}Ne−DMS	^{22}Ne−DMS
$A(0^+)$/MHz	5903.0241(54)	5901.2603(23)[b]
$A(0^-)$/MHz	5902.9946(54)	
$B(0^+)$/MHz	2132.50843(62)	2005.6408(12)
$B(0^-)$/MHz	2132.45528(62)	2005.6016(12)
$C(0^+)$/MHz	1821.62885(56)	1728.2105(12)
$C(0^-)$/MHz	1821.63880(56)	1728.2186(12)
$\Delta_J(0^+)$/kHz	44.835(17)	40.25(5)
$\Delta_J(0^-)$/kHz	44.648(17)	40.11(5)
$\Delta_{JK}(0^+)$/kHz	366.9(3)	327.4(8)
$\Delta_{JK}(0^-)$/kHz	362.3(3)	323.2(8)
$\Delta_K(0^+)$/kHz	−329.6(13)	−297.4(9)
$\Delta_K(0^-)$/kHz	−319.5(13)	−282.8(9)
$\delta_J(0^+)$/kHz	6.224(13)	5.16(5)
$\delta_J(0^-)$/kHz	6.137(13)	5.16(5)
$\Phi_{JK}(0^+)$/kHz	−1.978(8)	−1.470(25)
$\Phi_{JK}(0^-)$/kHz	−1.977(8)	−1.500(25)
$\Phi_{KJ}(0^+)$/kHz	7.40(7)	5.75(16)
$\Phi_{KJ}(0^-)$/kHz	6.77(7)	5.12(16)
$\phi_K(0^+)$/kHz	−32.20(9)	−28.44(27)
$\phi_K(0^-)$/kHz	−31.42(9)	−27.84(27)
L_J/Hz[b]	−0.045(6)	−0.18(7)
ΔE/MHz[c]	1.638(4)	1.413(2)
N[d]	68	46
$\Delta\nu_{rms}$/kHz[e]	3.87	3.74

[a] Errors in parentheses are a priori errors reported by SPFIT. [b] The average value of these constants for the two states was fitted. [c] ΔE is the energy difference between the 0^+ and 0^- tunneling substates. [d] N is the number of fitted transitions. [e] $\Delta\nu_{rms} = [\sum(\nu_{obs} - \nu_{calc})^2/N]^{1/2}$.

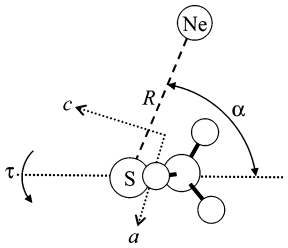

Figure 2. Definition of the structural parameters for the experimentally observed structure (II). R is the S···Ne distance; α locates the Ne atom in the bisector plane of the DMS, and τ is a torsional angle describing motion of the Ne atom around the C_2 axis of DMS: $\tau = 0°$ corresponds to a heavy atom planar structure whereas $\tau = 90°$ places the Ne above the DMS (in the σ_v plane bisecting the CSC angle). The MP2 calculations give a structure with an *ac* plane of symmetry with equilibrium values of $R = 3.850$ Å, $\alpha = 62.2°$, $\tau = 90°$.

TABLE 3: Structural Parameters from the Least-Squares Fitting Process[a]

parameter	structure II	structure II′
R(S···Ne)/Å	3.943(6)	3.571(8)
R_{CM}/Å	3.715(6)	3.715(8)
α/deg	63.2(6)	99.6(7)
std dev/u Å^2	0.2946	0.2946

[a] Structural parameters are defined in Figure 2. Structure II resembles that of Figure 2 with the Ne atom shifted toward the methyl groups whereas II′ locates the Ne atom more over the S atom (see Figure 3). Uncertainties show one standard deviation.

Dipole Moment. The dipole moment was determined from Stark effect measurements carried out on the lower tunneling components of several transitions (Table 4). The calculated Stark coefficients were obtained from perturbation theory using the fitted rotational constants given in Table 2 and neglecting cross terms between the two tunneling states. Observed Stark coefficients were least-squares fitted to obtain the μ_a and μ_c dipole moment components (Table 4). Observed Q-branch transitions had very fast Stark shifts due to large M^2E^2 terms, restricting us to measurement of R branch *c*-type or the considerably weaker *a*-type transitions. The μ_a dipole component is determined to be small ($\mu_a = 0.29(5)$ D), consistent with the much lower intensity of the *a*-type transitions. The total dipole moment of the complex, $\mu_{total} = 1.521(17)$ D, shows virtually no enhancement relative to the dipole moment of the DMS monomer (1.50(1) D).[25] This small change upon complexation is in qualitative agreement with the ab initio total dipole moment $\mu_{total} = 1.61$ D, of structure II, which is equal to that of the DMS monomer calculated at the same level ($\mu_{total} = 1.61$ D). It should be noted that because only lower tunneling components for the *c*-type transitions were included in the dipole moment data, some caution is warranted; however, the good agreement of observed and calculated Stark coefficients is sufficient to justify the neglect of the cross terms. In addition, semiquantitative Stark measurements of upper frequency components of the tunneling doublets at selected electric field strengths revealed identical shifts to those obtained for the lower frequency components.

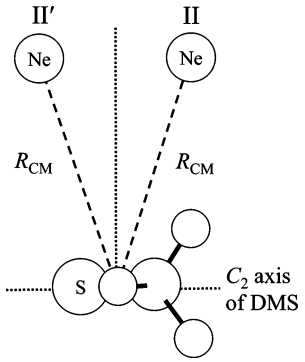

Figure 3. Two possible structures of the Ne−DMS dimer that are consistent with the inertial data. The two structures differ by the placement of the Ne atom with respect to the perpendicular to the C_2 axis of DMS (shown by the vertical dashed line) which originates at the center of mass of the DMS monomer.

TABLE 4: Measured Stark Coefficients and Dipole Moment Components for the ^{20}Ne−DMS Isotopomer[a]

transition	$\|M\|$	$\Delta\nu/E^2$ (obs)	$\Delta\nu/E^2$ (calc)	% diff
$1_{10} \leftarrow 0_{00}$	0	3.2562	3.3420	−2.6
$2_{11} \leftarrow 1_{01}$	0	0.7717	0.8266	−7.1
	1	4.4337	4.2934	3.2
$2_{12} \leftarrow 1_{11}$	0	0.2889	0.3035	−5.4
$3_{03} \leftarrow 2_{11}$	1	−0.5453	−0.5316	2.5
	2	−2.4554	−2.5251	−2.8
$3_{13} \leftarrow 2_{12}$	0	−0.7112	−0.7119	−0.1
	1	−1.0108	−1.0988	−8.7
		$\mu_a = 0.29(5)$ D		
		$\mu_c = 1.494(15)$ D		
		$\mu_{total} = 1.521(17)$ D		

[a] Stark coefficients are in units of 10^{-5} MHz V^{-2} cm^2.

Ab Initio Structure, Inversion Pathway and Barrier. Ab initio optimizations using Gaussian 98[26] at the MP2/6-311++G-(2d,2p) level (which gave a good quantitative description of the structure of the Ne-dimethyl ether complex[6]) allowed the identification of several stationary points on the potential energy surface; these structures (numbered I−VI) are shown in Figure 1 and are labeled in order of decreasing stability. Only structure II is consistent with the experimental rotational constants, planar moments and isotopic shifts.

Inclusion of zero-point energy (ZPE) corrections to the energies of the optimized stationary points causes a change in the relative stabilities (see Table 5): uncorrected, the structure

TABLE 5: Relative Energies (cm^{-1}) Obtained from MP2/6-311++G(2d,2p) Optimizations for the Structures I−VI of the Ne−DMS Dimer (see Figure 1)

structure	relative energy (uncorrected)	relative energy (ZPE corrected)
I	0.0	4.0
II	3.8	7.9
III	6.7	0.0
IV	17.7	9.9
V	23.3	19.8
VI	88.2	49.6

with the Ne located above the DMS, but situated just out of the symmetry plane (structure I) is given as the lowest energy structure; structure II (with the Ne in the σ_v plane that bisects the DMS) is only 3.8 cm^{-1} higher and the C_{2v} structure in which the Ne is located between the methyl groups (structure III) is a further 2.9 cm^{-1} higher in energy. Comparison of the ZPE corrected energies shows structure III to be the lowest energy structure, followed by I (4.0 cm^{-1} higher in energy) and then II (a further 3.9 cm^{-1} less stable). The order of stability of the remaining structures IV−VI is unchanged upon inclusion of ZPE corrections. Given the closeness of the energies in these calculations it is not possible to determine unambiguously the lowest energy geometry or the tunneling pathway from the computational results alone. However, the experimental planar moments are consistent with the Ne atom being located in the bisector plane of the DMS (as discussed above), so we favor II as the experimentally observed minimum. Comparison of the structural parameters of structure II from the ab initio calculations with the experimental values (Table 3) shows remarkably good agreement. The S···Ne bond distance is underestimated by about 2.5% (3.850 Å vs 3.943(6) Å) by the calculation and the angular agreement is similarly good (62.2° vs 63.2(6)°).

In addition to the full structural optimizations which identified the six stationary points described above, a series of partial optimizations were also carried out at the MP2/6-311++G(2d,2p) level to enable construction of a two-dimensional surface. This surface illustrates the energetic relationships between each stationary point and provides a means for identification of possible tunneling pathways. The angles α and τ (Figure 2) were varied in 15° increments, α from −180° to +180°, and τ from 0° to 180°. The distance between the Ne atom and the S atom of DMS was optimized at each (α, τ) coordinate in the potential energy scan; this distance showed a wide variation, from 3.85 Å in structure II to 4.53 Å in structure III. No corrections were made for basis set superposition error (BSSE) or zero point energy (ZPE) in the PES calculation. The resulting surface is shown in Figure 4, from which at least three possible pathways between the two equivalent structures II (which correspond to the Ne atom located on one side or the other of the DMS plane) can be recognized. The first of these (II−I−IV−I−II) involves passing through a C_s intermediate, IV, and hence requires negotiating four maxima. The second pathway (II−III−II) passes through the C_{2v} intermediate, III, and negotiates only two (lower energy) barriers. The differences in energy between the structures involved in both of these motions are very small (<10 cm^{-1} at this level of calculation), although detailed analysis of the motions is complicated by the fact that the relative stabilities of structures II and III change upon inclusion of ZPE corrections. The third motion (II−VI−II) involves a second C_{2v} intermediate, VI, but given the much larger difference in energy between the two species, the correspondingly higher barriers (∼90 cm^{-1} uncorrected, ∼50 cm^{-1} (ZPE corrected)), and the larger angular range traveled, it seems reasonable to eliminate this as the possible inversion

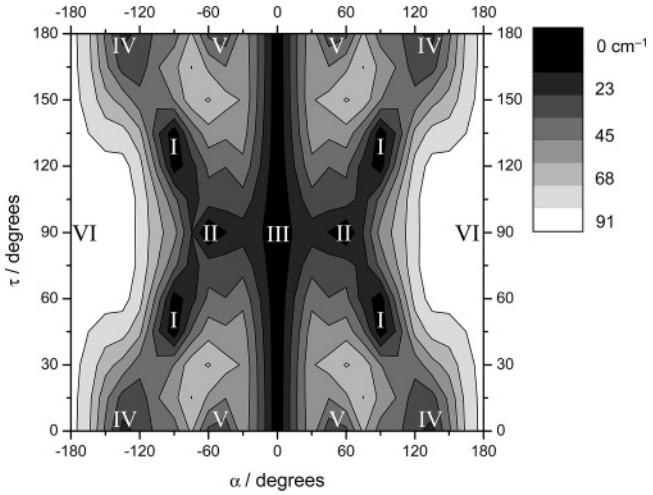

Figure 4. Two-dimensional potential energy surface calculated at the MP2/6-311++G(2d,2p) level showing the variation in total energy as a function of α and τ (see Figure 2). The local minima are shown as the darkest regions, and labeled I−VI; contours are labeled in units of cm^{-1} relative to the minimum energy structure. The energies are uncorrected for ZPE and BSSE.

pathway. Interestingly, in the case of the Ne−DME[6,11] and Ar−DME[11,27] complexes, the tunneling motion was determined to be via a planar intermediate similar to the C_s symmetry structure IV. In contrast, for the DME−Kr[28] complex, the proposed tunneling motion involved a C_{2v} structure (analogous to VI) as the intermediate, which is predicted to be a much higher energy (less favorable) motion in the case of Ne−DMS.

Discussion

Comparison of the structure of Ne−DMS to that of the analogous Ne−DME complex reveals that the Ne atom is shifted further back toward the methyl groups in the DMS complex. This might be understood at the most simplistic level by examination of the van der Waals radii of the central S or O atom in the two complexes (R_{vdW}(O) = 1.40 Å, R_{vdW}(S) = 1.85 Å).[29] The larger S atom in DMS forces the Ne to be situated further away from the central atom, toward the CH_3 groups at an R(S···Ne) distance of 3.943(6) Å and an angle α(cm···S···Ne) of 63.2(6)° (Figure 2). This is in contrast to the Ne−DME complex,[6] where the experimental R(O···Ne) distance was found to be 3.19(1) Å and α(cm···O···Ne) was 115(1)° (r_0 geometry). Inspection of the intermolecular distances in structure II for Ne−DMS reveals that the Ne is almost equidistant from the heavy atoms of the DMS (S···Ne = 3.94 Å and C···Ne = 3.83 Å), thereby maximizing the dispersion interactions.

Although ab initio optimizations and calculation of a potential energy surface for the Ne−DMS complex have shown that there are several stationary points that are very close in energy, from Figure 4 it is difficult to specify unambiguously what the tunneling pathway is. This level of calculation indicates that the most likely tunneling motion of the Ne atom is either through the C_{2v} transition state with the Ne located between the methyl groups of DMS (structure III), which can be pictured as a motion principally involving the α coordinate, or through the C_s structure, IV (which can be imagined as a motion of the τ coordinate). In either case, the barriers that need to be surmounted are predicted from the PES to be small (∼20 cm^{-1} in the first case and ∼40 cm^{-1} in the second). The motion through structure VI requires surmounting a higher barrier of ∼90 cm^{-1} and also requires a much larger angular motion

(∼240°); in light of these factors this seems to be a lower probability pathway for the inversion motion. The rather low ab initio estimates of the barrier do seem inconsistent with the small experimental inversion splitting ($\Delta E(^{20}\text{Ne}-\text{DMS}) = 1.638(4)$ MHz); perhaps the tunneling frequency is reduced considerably in light of the large angular separation of the minima (II), 126° in the case of the pathway II−III−II and 180° in pathway II−I−IV−I−II. Alternatively, the ab initio calculations may just dramatically underestimate the barrier height for this complex. This would be in contrast to the Ne−DME[6] and Ar−DME[27] complexes where similar MP2 calculations overestimated the barrier to inversion.

Given the crudeness of the potential energy surface and the fact that the relative stabilities change upon inclusion of ZPE, attempts to obtain a barrier using a one-dimensional model such as that of Meyer[30] were not pursued. Nevertheless, the PES calculations have proven useful for a qualitative examination of the possible tunneling pathways. It should be stressed that the effects of basis set superposition error (BSSE) were neglected in the calculation of our PES, and it is likely that higher level calculations utilizing larger basis sets to improve modeling of the dispersion interactions and to reduce the effects of BSSE, may offer a more accurate quantitative picture of the energetics and inversion pathway.

Conclusions

The structure of the Ne−DMS weak complex has been determined to be of C_s symmetry and possesses an inversion motion that allows the Ne atom to tunnel from one side of the DMS plane to the other. Our MP2/6-311++G(2d,2p) calculations indicate a barrier to this inversion motion of between 20 and 40 cm^{-1}, depending on the tunneling pathway. Despite the approximations made in the current work, we feel that the PES identifies the important stationary points and provides a qualitative picture of the tunneling pathways and we propose that the quoted values of the inversion barrier be viewed as a lower bound to the true figure.

Acknowledgment. S.A.P. acknowledges the Donors of the American Chemical Society Petroleum Research Fund for partial support of this work (PRF #39752-GB6).

References and Notes

(1) Novick, S. E. *Bibliography of Rotational Spectra of Weakly Bound Complexes* **2005**. Electronic updates are available on the web at http://www.wesleyan.edu/chem/faculty/novick/vdw.html.

(2) LoBue, J. M.; Munrow, M.; Novick, S. E. 1998, unpublished results.

(3) Enami, S.; Nakano, Y.; Hashimoto, S.; Kawasaki, M.; Aloisio, S.; Francisco, J. S. *J. Phys. Chem. A* **2004**, *108*, 7785.

(4) A brief list of DME complexes is given in: Peebles, S. A.; Peebles, R. A.; Newby, J. J.; Serafin, M. M. *Chem. Phys. Lett*. **2005**, *410*, 77.

(5) Tatamitani, Y.; Bingxin, L.; Shimada, J.; Ogata, T.; Ottaviani, P.; Maris, A.; Caminati, W.; Alonso, J. L. *J. Am. Chem. Soc*. **2002**, *124*, 2739.

(6) Maris, A.; Caminati, W. *J. Chem. Phys*. **2003**, *118*, 1649.

(7) Balle, T. J.; Flygare, W. H. *Rev. Sci. Instrum*. **1981**, *52*, 33.

(8) Hillig, K. W.; Matos, J.; Scioly, A.; Kuczkowski, R. L. *Chem. Phys. Lett*. **1987**, *133*, 359.

(9) Newby, J. J.; Serafin, M. M.; Peebles, R. A.; Peebles, S. A. *Phys. Chem. Chem. Phys*. **2005**, *7*, 487.

(10) Kawashima, Y.; Ohashima, Y.; Endo, Y. *Chem. Phys. Lett*. **1999**, *315*, 201.

(11) Morita, Y.; Ohashi, N.; Kawashima, Y.; Hirota, E. *J. Chem. Phys*. **2006**, *124*, 094301.

(12) Muenter, J. S. *J. Chem. Phys*. **1968**, *48*, 4544.

(13) Xu, Y.; Jäger, W. *J. Chem. Phys*. **1997**, *106*, 7968.

(14) Xu, Y.; Jäger, W. *J. Chem. Phys*. **1997**, *107*, 4788.

(15) Ngari, M. S.; Jäger, W. *J. Chem. Phys*. **1999**, *111*, 3919.

(16) Xu, Y.; Jäger, W. *Phys. Chem. Chem. Phys*. **2000**, *2*, 3549.

(17) Niide, Y.; Hayashi, M. *J. Mol. Spectrosc*. **2003**, *220*, 65.

(18) Pickett, H. M. *J. Mol. Spectrosc*. **1991**, *148*, 371.

(19) Watson, J. K. G. In *Vibrational Spectra and Structure*; Durig, J. R., Ed.; Elsevier: New York/Amsterdam, 1977; Vol. 6, p 1.

(20) Pickett, H. M. *J. Chem. Phys*. **1972**, *56*, 1715.

(21) Schwendeman, R. H. In *Critical Evaluation of Chemical and Physical Structural Information*; Lide, D. R., Paul, M. A., Eds.; National Academy of Sciences: Washington, DC, 1974.

(22) Kraitchman, J. *Am. J. Phys*. **1953**, *17*, 21.

(23) Millen, D. J. *Can. J. Chem*. **1985**, *63*, 1477.

(24) Balle, T. J.; Campbell, E. J.; Keenan, M. R.; Flygare, W. H. *J. Chem. Phys*. **1980**, *72*, 922.

(25) Pierce, L.; Hayashi, M. *J. Chem. Phys*. **1961**, *35*, 479.

(26) Frisch, M. J.; Trucks, G. W.; Schlegel, H. B.; Scuseria, G. E.; Robb, M. A.; Cheeseman, J. R.; Zakrzewski, V. G.; Montgomery, J. A.; Stratmann, R. E.; Burant, J. C.; Dapprich, S.; Millam, J. M.; Daniels, A. D.; Kudin, K. N.; Strain, M. C.; Farkas, O.; Tomasi, J.; Barone, V.; Cossi, M.; Cammi, R.; Mennucci, B.; Pomelli, C.; Adamo, C.; Clifford, S.; Ochterski, J.; Petersson, G. A.; Ayala, P. Y.; Cui, Q.; Morokuma, K.; Malick, D. K.; Rabuck, A. D.; Raghavachari, K.; Foresman, J. B.; Cioslowski, J.; Ortiz, J. V.; Baboul, A. G.; Stefanov, B. B.; Liu, G.; Liashenko, A.; Piskorz, P.; Komaromi, I.; Gomperts, R.; Martin, R. L.; Fox, D. J.; Keith, T.; Al-Laham, M. A.; Peng, C. Y.; Nanayakkara, A.; Challacombe, M.; Gill, P. M. W.; Johnson, B. G.; Chen, W.; Wong, M. W.; Andres, J. L.; Gonzalez, C.; Head-Gordon, M.; Replogle, E. S.; Pople, J. A. *Gaussian 98*, revision A.9; Gaussian, Inc.: Pittsburgh, PA, 1998.

(27) Ottaviani, P.; Maris, A.; Caminati, W.; Tatamitani, Y.; Suzuki, Y.; Ogata, T.; Alonso, J. L. *Chem. Phys. Lett*. **2002**, *361*, 341.

(28) Velino, B.; Melandri, S.; Caminati, W. *J. Phys. Chem. A* **2004**, *108*, 4224.

(29) Pauling, L. *College Chemistry*, 3rd ed.; W. H. Freeman and Co.: San Francisco, 1964; p 290.

(30) Meyer, R. *J. Mol. Spectrosc*. **1979**, *76*, 266.